Quaternary Research 82 (2014) 236–248

Contents lists available at ScienceDirect

Quaternary Research

journal homepage: www.elsevier.com/locate/yqres

Millennial-scale variations in western Sierra Nevada precipitation during the last glacial cycle MIS 4/3 transition

Jessica L. Oster [a,*], Isabel P. Montañez [b], Regina Mertz-Kraus [c,1], Warren D. Sharp [c], Greg M. Stock [d], Howard J. Spero [b], John Tinsley [e], James C. Zachos [f]

[a] Earth and Environmental Sciences, Vanderbilt University, USA
[b] Earth and Planetary Sciences, University of California, Davis, USA
[c] Berkeley Geochronology Center, USA
[d] National Park Service, Yosemite National Park, USA
[e] US Geological Survey, Menlo Park, CA, USA
[f] Earth and Planetary Sciences, University of California, Santa Cruz, USA

ARTICLE INFO

Article history:
Received 14 August 2013
Available online 10 May 2014

Keywords:
Speleothem
Sierra Nevada
Dansgaard–Oeschger cycles
MIS 3
MIS 4

ABSTRACT

Dansgaard–Oeschger (D–O) cycles had far-reaching effects on Northern Hemisphere and tropical climate systems during the last glacial period, yet the climatic response to D–O cycles in western North America is controversial, especially prior to 55 ka. We document changes in precipitation along the western slope of the central Sierra Nevada during early Marine Oxygen Isotope Stages (MIS) 3 and 4 (55–67 ka) from a U-series dated speleothem record from McLean's Cave. The timing of our multi-proxy geochemical dataset is coeval with D–O interstadials (15–18) and stadials, including Heinrich Event 6. The McLean's Cave stalagmite indicates warmer and drier conditions during Greenland interstadials (GISs 15–18), signified by elevated $\delta^{18}O$, $\delta^{13}C$, reflectance, and trace element concentrations, and less radiogenic $^{87}Sr/^{86}Sr$. Our record extends evidence of a strong linkage between high-latitude warming and reduced precipitation in western North America to early MIS 3 and MIS 4. This record shows that the linkage persists in diverse global climate states, and documents the nature of the climatic response in central California to Heinrich Event 6.

Introduction

Irregular, millennial-scale climate fluctuations known as Dansgaard–Oeschger (D–O) cycles are prominent features of Marine Oxygen Isotope Stages (MIS) 4, 3, and 2 (73.5–17.8 ka). First identified in the Greenland ice-core records (e.g. Dansgaard et al., 1984; Johnsen et al., 1992), D–O cycles are characterized by abrupt temperature increases of up to 10°C in as little as 50 yrs, followed by gradual cooling, and terminating in brief periods of accelerated cooling and cold conditions in the North Atlantic (Steffensen et al., 2008; Wolff et al., 2010). The most prominent of these abrupt terminal coolings are associated with Heinrich Events, large discharges of icebergs that are inferred from an influx of detrital grains in North Atlantic sediment cores (Heinrich, 1988).

High-resolution paleoclimate proxy records document the response of the Intertropical Convergence Zone (ITCZ) (Peterson et al., 2000) and East Asian (Wang et al., 2001; Cheng et al., 2009) and South American monsoons (Wang et al., 2007; Kanner et al., 2012) to D–O cycles and Heinrich Events across MIS 2 through 4 and beyond. However, few continuous records with sufficient resolution to capture D–O variability have been developed for terrestrial mid-latitude regions outside the direct influence of the ITCZ and monsoon systems (Voelker and workshop participants, 2002; Genty et al., 2003; Harrison and Sanchez Goñi, 2010; Jo et al., 2014). Two speleothem $\delta^{18}O$ records from the southwestern United States reveal a strong regional correlation with D–O events during MIS 2 and 3, interpreted to reflect elevated winter precipitation during Greenland stadials (cold periods) and reduced winter precipitation during interstadials (warm periods) (Asmerom et al., 2010; Wagner et al., 2010). Less is known about the relationship between D–O cycles, Heinrich events and western North American climate prior to MIS 3 (~55 ka), a time period that is especially difficult to investigate given that it is beyond radiocarbon age control. Lake records from the Great Basin suggest shifts to colder and wetter conditions during Heinrich Events, including the oldest Heinrich Event 6 (H6) (Bischoff and Cummins, 2001; Jiménez-Moreno et al., 2007). In contrast, the Devils Hole $\delta^{18}O$ record, which apparently has resolution adequate to capture D–O events during MIS 3 and 4, does not display millennial-

* Corresponding author at: 5726 Stevenson Center, 7th Floor, Nashville, TN 37240, USA.
E-mail address: jessica.l.oster@vanderbilt.edu (J.L. Oster).
[1] Present address: Institute for Geosciences, Johannes Gutenberg University, Mainz, Germany.

http://dx.doi.org/10.1016/j.yqres.2014.04.010
0033-5894/

scale variability consistent with D–O cycles and Heinrich Events (Winograd et al., 2006). Thus, it remains unclear how (and if) climate in western North America varied in response to these events prior to 55 ka.

Stalagmites from caves on the western slope of the central Sierra Nevada provide proxy records of past precipitation (Oster et al., 2009, 2010) with sufficient continuity and temporal resolution to assess climatic responses to D–O cycles and Heinrich Events. Here, we present U-series-dated records of growth rate, reflectance, stable isotope and $^{87}Sr/^{86}Sr$ ratios, and trace elements from a stalagmite from McLean's Cave, California (Fig. 1), a ~290 mm segment of which grew from 67 to 55 ka. Stable and radiogenic isotope and reflectance records from McLean's Cave share many features coincident with millennial-scale climate events, including D–O cycles, documented in time-equivalent Greenland ice-core records (Dansgaard et al, 1984; NGRIP Members, 2004), Cariaco Basin sediments (Peterson et al., 2000), and Chinese, Brazilian, and European speleothems (Wang et al., 2001, 2004, 2007; Genty et al., 2003). Our new record also documents a significant climate response in central California to H6 and provides new constraints on the timing and duration of the effects of H6 in the mid latitudes. The McLean's Cave stalagmite provides the first precisely dated record of the dynamic and variable climate in western North America that prevailed during MIS 4 and early MIS 3.

Site and sample description

McLean's Cave (Fig. 1) is developed within the Columbia carbonate lens, one of several discrete metamorphosed pre-Jurassic limestone and dolomite masses in the Sierra Nevada foothills that are tectonically intercalated with other metasedimentary and metavolcanic rocks of the Calaveras Complex (Clark and Lydon, 1962; Bowen, 1973). The Columbia carbonate lens is oriented NE–SW and is 6.5 km long by 2.4–4 km wide (Clark and Lydon, 1962). The cave entrance, which is 300 m above sea level (asl), is located near the bottom of the South Fork Stanislaus River canyon. Speleothem ML-2, a ~400 mm long stalagmite, was collected in 1979 from the upper passage of McLean's Cave, below 30–60 m of carbonate bedrock (Fig. 1C), just prior to cave inundation following construction of the New Melones Dam.

The climate above McLean's Cave is characterized by cool, wet winters and warm, dry summers. From 1951 to 2011, a University of California weather station located 11.2 km southeast of McLean's Cave at 533 m asl, experienced an average annual precipitation of ~850 mm. On average, 93% of this precipitation occurred between October and April. Only 2% of annual precipitation fell between July and September, suggesting minor influence by localized summer convective storms. McLean's Cave is not significantly influenced by precipitation related to the North American Monsoon (Higgins et al., 1999).

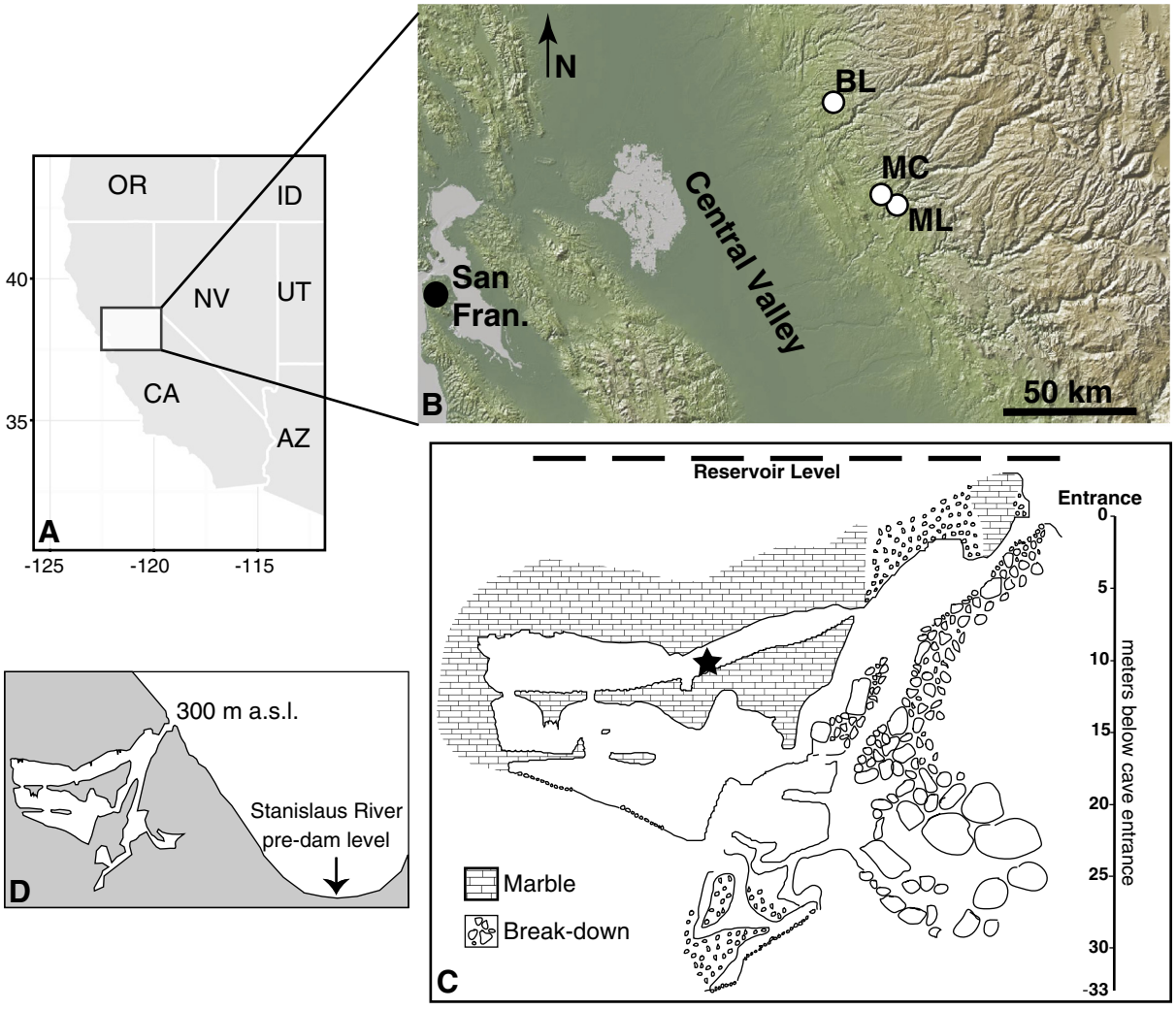

Figure 1. Location of McLean's Cave (ML; 38°4.20′N, 120°25.20 W; elevation of 300 m asl) in the western United States (A) and the western foothills of the Sierra Nevada (B) with location of Black Chasm Cavern (BL; Oster et al., 2012) and Moaning Cave (MC; Oster et al., 2009). (C) Cross-sectional view of McLean's Cave (adapted from McEachern and Grady, 1978). Star shows location of sample ML-2 at time of collection. (D) Cross-sectional location of the cave in relation to level of the Stanislaus River prior to construction of the New Melones Dam.

https://doi.org/10.1016/j.yqres.2014.04.010 Published online by Cambridge University Press

Daily average temperature is 22.7°C during the summer (June–September) and 7.6°C during the winter (November–February). Present vegetation in this area consists of C_3 plants, including manzanita (*Arctostaphylos* sp.), toyon (*Heteromeles arbutifolia*), and other chaparral species, and there is no evidence of transitions to C_4 plant assemblages during the Pleistocene in this region (Cole, 1983; Davis, 1999).

Methods

U-series

Twelve U–Th dating samples were drilled from ML-2 following visible growth bands (Fig. 2). A ~1 mm wide dark band signifies a hiatus 85 mm below the top of the stalagmite. Dating of material on either side of this dark band indicates a growth hiatus occupying most of the glacial period between 55.7 ± 0.52 and 16.7 ± 2.55 ka. More recent calcite growth above this hiatus is porous and incorporates abundant detrital material, so dating efforts and geochemical analyses were focused on the older material.

Analyses were performed at the Berkeley Geochronology Center first using a Micromass Sector-54 Thermal Ionization Mass Spectrometer (TIMS) and then a Thermo NEPTUNE *Plus* Multi-Collector-Inductively-Coupled-Mass-Spectrometer (MC-ICP-MS). Samples of ~750–3300 mg for TIMS and ~200 mg for MC-ICP-MS were totally dissolved in 7 N HNO_3 and equilibrated with a mixed spike containing ^{229}Th, ^{233}U, and ^{236}U. The spike was calibrated against solutions of NBL CRM 145 and solutions prepared from a 69 Ma U ore that has been demonstrated to yield concordant U/Pb ages (Schwartzwalder Mine, Colorado, USA; hereafter, SM; Ludwig et al., 1985) and sample-to-sample agreement of $^{234}U/^{238}U$ and $^{230}Th/^{238}U$ ratios. U and Th were separated using two stages of HNO_3–HCl cation exchange chemistry followed by reaction with HNO_3 and $HClO_4$ to remove any residual organic material. MC-ICP-MS analyses followed the procedures outlined in Mertz-Kraus et al. (2012). Measured peak heights were corrected for multiplier dark noise/Faraday baselines, background intensities, ion counter yields, tail contributions, and interfering spike isotopes. Mass fractionation was determined using the gravimetrically determined $^{233}U/^{236}U$ ratio of the spike. The external reproducibility of $^{234}U/^{238}U$ and $^{230}Th/^{238}U$ ratios of SM solutions measured during each run was better than 0.2%. Ages were calculated using the half-lives of Jaffey et al., (1971) for ^{238}U, Holden (1990) for ^{232}Th, and Cheng et al. (2000) for ^{230}Th and ^{234}U. Measured $^{230}Th/^{232}Th$ activity ratios, which scale with contamination by detritus, range from about 10 to 830 (median = 66), indicating that some samples require significant correction for U and Th from detritus. Correction was made assuming activity ratios of ($^{232}Th/^{238}U$) = 1.2 ± 0.6, ($^{230}Th/^{238}U$) = 1.0 ± 0.1, and ($^{234}U/^{238}U$) = 1.0 ± 0.1, which correspond to average silicate crust in secular equilibrium. An isochron constructed for five fractions of sample ML12, though somewhat scattered (MSWD = 6.5), yielded an age of 55.4 ± 1.2 ka. This age is in good agreement with the mean corrected age of this sample (55.70 ± 0.49 ka), indicating that the detritus correction is appropriate. Age uncertainties are stated at the 2σ level and include measurement errors as well as uncertainties associated with the initial isotope correction.

An age-depth model for ML-2 was constructed using the StalAge algorithm of Scholz and Hoffmann (2011). Comparison of StalAge and other modeling approaches using both synthetic and natural data sets, demonstrated that it performs well in dealing with complexities such

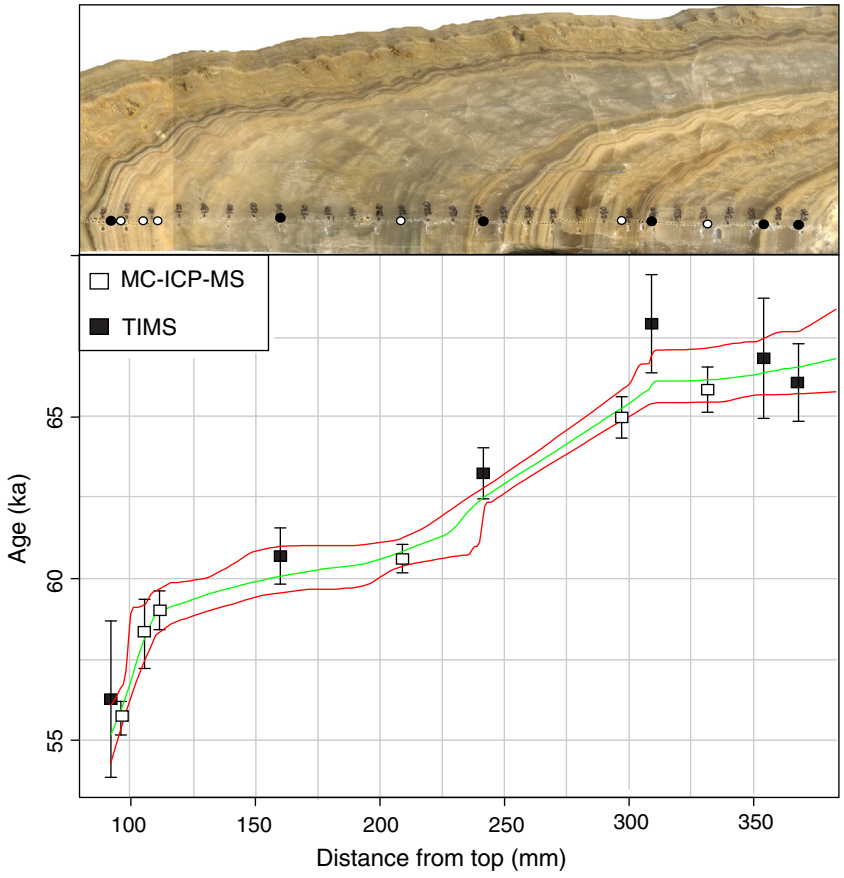

Figure 2. Photograph of stalagmite ML-2 (top) with sample locations for U-series dating marked by circles (closed circles: TIMS, open circles MC-ICP-MS). U-series ages versus depth (bottom) with associated 2σ errors analyzed by TIMS (closed squares) and MC-ICP-MS (open squares). Age model for ML-2 was computed using the StalAge algorithm in R (Scholz and Hoffmann, 2011). Green line shows the final age model and red lines show associated 95% confidence limits.

https://doi.org/10.1016/j.yqres.2014.04.010 Published online by Cambridge University Press

as outliers, age inversions, large and abrupt changes in growth rate, and hiatuses that are found in many speleothem time series constrained by ^{230}Th/U dating (Scholz et al., 2012). We selected StalAge for our study because it considers stratigraphic information in addition to ages and their assigned uncertainties, is objective, can be applied to data sets containing large changes in growth rate, performs well when applied to synthetic data sets where the "true" age model is known, and accounts for complexities by increasing the uncertainties assigned to the age model.

Stable isotope compositions and reflectance measurements

Using a binocular microscope and modified dental drill, 370 samples weighing ~10 μg each were taken at 1 mm intervals along the central growth axis of ML-2. Samples were baked at 100°C under vacuum for 30 min to drive off water vapor, reacted in 105% orthophosphoric acid at 90°C, and analyzed using either a PRISM or an OPTIMA gas source isotope ratio mass spectrometer at the University of California Santa Cruz. Analytical precision based on replicate analyses of in house standard (CM) was better than ±0.05 and 0.1‰ (1σ) for C and O respectively. Oxygen and carbon isotope ratios are expressed relative to VPDB.

Reflectance data for ML-2 were obtained using high-resolution flatbed scanner imaging, sampling along the central growth axis of the stalagmite. Using the software NIH Image (http://rsb.info.nih.gov/nih-image/), a single pixel profile was generated along the growth axis of the ML-2 approximately 1 pixel width from the stable isotope sampling transect. This profile was converted to grayscale values where 0 represents black and the maximum value of 255 corresponds to white. Grayscale values and variations were reproducible along multiple profiles within several pixels of the stalagmite growth axis.

Strontium isotopes and trace elements

Three to six mg of calcite from ML-2, sampled at 1–2 mm intervals, and host calcite and dolomite marbles taken from the Columbia Quarry directly across the South Fork of the Stanislaus River from McLean's Cave, were processed for Sr isotope analysis. Strontium was isolated using Eichrom Sr Spec cation exchange resin (Horwitz et al., 1992). ^{87}Sr/^{86}Sr ratios were measured in solution mode on a Nu Instruments Multi-Collector-Inductively Coupled Plasma Mass Spectrometer (MC-ICP-MS) in the Earth and Planetary Sciences Department at the University of California, Davis. The measured ^{87}Sr/^{86}Sr ratio of NIST SRM 987 was 0.710251 ± 0.000025 (2σ, n = 30) during this study. All measured sample ^{87}Sr/^{86}Sr ratios were normalized to a nominal value for NIST SRM 987 of 0.710248. A modern coral from the South China Sea was used as an in-house consistency standard. Its value for the measurement period was 0.709183 ± 0.000040 (2σ, n = 10), which falls within the range of modern seawater ^{87}Sr/^{86}Sr (0.70916–0.70923) (DePaolo and Ingram, 1985; Palmer and Edmond, 1989).

Trace-element analyses conducted on a subsection of the ML-2 stalagmite (interval from 130 to 224 mm) were carried out using a New Wave Research UP-213 ablation system coupled to an Agilent 7500 series quadrupole ICP-MS at the Interdisciplinary Center for Plasma Mass Spectrometry, UC Davis. This interval was analyzed because it covers a prominent shift in stalagmite δ^{13}C. We analyzed a polished thick section (~400 μm) at 70% laser energy and 10 Hz using a spot size of 20 μm and spacing of 150 μm. We used the multi-element synthetic glass NIST SRM 612 for calibration of the element concentrations, and the preferred values reported in the GeoReM database (http://georem.mpch-mainz.gwdg.de/) (Jochum et al., 2011) as the "true" concentrations in the reference glass. Data were reduced using the program GLITTER (www.glitter-gemoc.com). USGS MACS-3, a synthetic calcium carbonate was used as a matrix-matched quality control material. Concentrations determined for USGS MACS-3 during this study were compared to the recommended values of the preliminary Certificate of the USGS (2010). The measured values for USGS MACS-3 agree within 11% for Mg, 4% for Sr, and 8% for Ba with the certified values. Precision (2σ, n = 71) on the MACS-3 measurements was 17% for Mg, 13% for Sr, and 11% for Ba throughout the course of the measurement period.

Statistical tests

In order to characterize the sign and strength of relationships among isotopic and geochemical proxies, Spearman rank-order correlation coefficients ("r_s") and one-tailed tests of significance ("p") between pairs of measured parameters were calculated using the statistics program R 2.15.1 (R Core Team, 2012). In order to calculate correlation coefficients between time-series of different resolution, proxy data were binned according to the median time step for the lower resolution data set and data within each bin was averaged. Linear trends were removed from the data sets prior to calculating r_s values in order to evaluate shorter-term correlations between parameters without the bias of long-term linear trends.

To facilitate visual comparison, higher-resolution (trace element) time-series were smoothed using a Gaussian kernel density estimation, a robust method for comparison of irregularly sampled time-series (Rehfeld et al., 2011). Kernel smoothing bandwidths were selected using the Sheather-Jones method (Sheather and Jones, 1991) included in the SiZer package in R (Sonderegger, 2011).

Results

U-series

Analytical results and calculated ages are given in Table 1. Measured U concentrations were relatively low, ranging from 46 to 65 ppb (median = 53 ppb). U-series ages for the ML-2 stalagmite preserve stratigraphic order within dating errors (Table 1; Fig. 2). Corrected U-series ages for ML-2 below its growth hiatus range from 67.80 ± 1.5 to 55.70 ± 0.49 ka, indicating that our proxy records span the transition between MIS 4 and 3 at 59.44 ± 1.287 (Wolff et al., 2010).

Stable isotope compositions and reflectance

The McLean's Cave stalagmite δ^{13}C time-series exhibits systematic fluctuations between −11.8‰ and −5.9‰, while δ^{18}O displays a smaller range of values between −11.0‰ and −8.1‰. Both datasets define similar trends (Fig. 3). Mickler et al. (2004, 2006) showed that non-equilibrium fractionation of stable isotopes can occur during speleothem growth due to rapid and extended degassing of CO_2 driven by decreased seepage-water flow rates, increased evaporation, and/or changing cave air–water CO_2 ratios. Such kinetic effects lead to ^{13}C- and ^{18}O-enrichment in the speleothem and elevated concentrations of trace elements such as Mg, Sr, and Ba (Lorens, 1981). As McLean's Cave has been inundated since 1979, it was not possible to collect modern calcite or drip water for calibration purposes. "Hendy Tests" have also been used to check for isotopic equilibrium during speleothem precipitation. A speleothem will pass the Hendy Test if δ^{18}O values remain constant along a growth layer and there is no relationship between δ^{18}O and δ^{13}C along the growth axis (Hendy, 1971). Three series of stable isotope measurements were performed along ML-2 growth bands. Variability in δ^{18}O along each band is 0.25, 0.32, and 0.63‰ respectively, and δ^{18}O and δ^{13}C are not significantly correlated along any of the bands (Supplementary Fig. 1). The results of the Hendy Tests suggest that the moderate down-axis correlation between δ^{18}O and δ^{13}C (r_s = 0.56; Table 2) is a result of environmental processes that influence both proxies independently rather than non-equilibrium calcite precipitation (e.g. Genty et al., 2003; Frappier et al., 2007; Oster et al., 2009).

McLean's Cave stalagmite reflectance varies between grayscale values of 58 and 248, with higher values corresponding to brighter areas of the stalagmite, and lower values corresponding to darker

https://doi.org/10.1016/j.yqres.2014.04.010 Published online by Cambridge University Press

Table 1
^{230}Th/U analytical data and ages for ML-2 speleothem.

Sample	Depth (mm)	Wt (mg)	U (ppm)	^{232}Th (ppm)	^{230}Th/^{232}Th	Measured ^{230}Th/^{238}U	Measured ^{234}U/^{238}U	Uncorrected Age (ka)	95% Conf. (ka)	Corrected Age (ka)	95% Conf. (ka)	Initial ^{234}U/^{238}U
ML17	83.0	202.5	0.0613	0.0106	3.416	0.1942 ± 0.0010	1.0831 ± 0.0052	21.49	±0.18	16.63	±2.55	1.0914 ± 0.0079
ML9	92.0	749.4	0.0481	0.00727	9.791	0.4884 ± 0.0071	1.1405 ± 0.0041	60.19	±1.19	56.20	±2.41	1.1717 ± 0.0076
ML12a	96.0	201.6	0.0497	0.00133	52.38	0.4580 ± 0.0023	1.1255 ± 0.0036	56.33	±0.45	55.64	±0.58	1.1479 ± 0.0042
ML12b	96.0	200.4	0.0499	0.00179	39.34	0.4604 ± 0.0018	1.1335 ± 0.0044	56.17	±0.42	55.25	±0.64	1.1576 ± 0.0052
ML12c	96.0	199.7	0.0469	0.00234	28.67	0.4690 ± 0.0022	1.1306 ± 0.0045	57.74	±0.48	56.45	±0.83	1.1553 ± 0.0056
ML12A-1	96.0	186.8	0.0482	0.000926	73.03	0.4608 ± 0.0026	1.1343 ± 0.0028	56.18	±0.45	55.68	±0.52	1.1580 ± 0.0033
ML12A-2	96.0	204.8	0.0460	0.00369	17.84	0.4703 ± 0.0018	1.1282 ± 0.0021	58.12	±0.33	56.01	±1.15	1.1536 ± 0.0038
ML18	105.5	201.5	0.0581	0.00431	19.79	0.4816 ± 0.0015	1.1256 ± 0.0024	60.40	±0.35	58.21	±1.07	1.1510 ± 0.0039
ML13	111.5	210.4	0.0564	0.00139	59.48	0.4802 ± 0.0023	1.1304 ± 0.0044	59.57	±0.50	58.94	±0.60	1.1550 ± 0.0052
ML2	160.0	1024.5	0.0644	0.00113	84.27	0.4884 ± 0.0031	1.1282 ± 0.0086	61.10	±0.84	60.62	±0.87	1.153 ± 0.010
ML14	209.0	210.5	0.0610	0.000108	832.2	0.4840 ± 0.0022	1.1252 ± 0.0032	60.58	±0.44	60.54	±0.44	1.1486 ± 0.0037
ML10	241.5	3332.7	0.0494	0.000206	365.2	0.5025 ± 0.0043	1.1302 ± 0.0039	63.30	±0.79	63.18	±0.79	1.1558 ± 0.0045
ML11	297.0	202.1	0.0650	0.000237	431.3	0.5117 ± 0.0030	1.1283 ± 0.0045	64.99	±0.64	64.90	±0.64	1.1542 ± 0.0053
ML7	309.0	960.5	0.0498	0.000740	108.8	0.5333 ± 0.0076	1.1348 ± 0.0080	68.17	±1.51	67.80	±1.52	1.1639 ± 0.0095
ML16	331.5	203.6	0.0541	0.000811	105.3	0.5188 ± 0.0028	1.1291 ± 0.0054	66.15	±0.67	65.76	±0.70	1.1561 ± 0.0063
ML8	354.0	950.0	0.0527	0.00151	56.40	0.5335 ± 0.0087	1.143 ± 0.012	67.51	±1.82	66.73	±1.86	1.175 ± 0.014
ML5	368.0	989.6	0.0582	0.000316	292.5	0.5239 ± 0.0043	1.140 ± 0.011	66.10	±1.20	65.98	±1.20	1.169 ± 0.013

All isotope ratios are given as activity ratios. Ages were corrected for initial isotopes using (^{232}Th/^{238}U) = 1.21 ± 0.5, (^{234}U/^{238}U) = 1.0 ± 0.1, and (^{230}Th/^{238}U) = 1.0 ± 0.1. Initial ^{234}U/^{238}U ratios were back-calculated using ages and measured ^{234}U/^{238}U ratios. Decay constants are those of Jaffey et al. (1971) for ^{238}U, Holden (1990) for ^{232}Th, and Cheng et al. (2000) for ^{230}Th and ^{234}U.

areas (Fig. 3D). The ML-2 stalagmite is dominated by columnar calcite textures (Kendall and Broughton, 1978; Frisia et al., 2000). Columnar calcite in speleothems initially forms as smaller acicular crystallites that coalesce into larger columnar composite crystals. Incomplete coalescence of crystallites can lead to the formation of elongated pores between crystallite boundaries that may contain water or air as inclusions (Kendall and Broughton, 1978), and the generation of an open columnar fabric (Frisia and Borsato, 2010). The reflectance signal of ML2 primarily indicates the density of these inclusions in the calcite and the presence of more open (high reflectance) or compact (low reflectance) calcite fabric (Supplementary Fig. 2). There are a few exceptions to this relationship. Several sub-mm scale detritus-rich bands between 303 and 307 mm depth in the stalagmite (at ~65.7 ka) cause sharp spikes in the reflectance profile. In addition, in the very youngest portion of the stalagmite studied, approximately 4 mm below the hiatus, higher reflectance corresponds to microcrystalline calcite textures (Frisia et al., 2000). Variations in reflectance correlate with long-term changes in stalagmite growth rate (Figs. 3D,F) and display moderate positive correlations with δ^{13}C and δ^{18}O (Table 2).

Strontium isotopes and trace elements

McLean's Cave stalagmite ^{87}Sr/^{86}Sr varies between 0.70715 and 0.70668 (Fig. 3). Calcite marble from the Columbia Quarry developed in the host carbonate unit has an average ^{87}Sr/^{86}Sr value of 0.707233 ± 0.000009 (1σ, n = 3), whereas dolomite marble is less radiogenic, with an average ^{87}Sr/^{86}Sr value of 0.706773 ± 0.00059 (1σ, n = 3).

McLean's Cave stalagmite trace element concentrations were measured for the interval 61.3 to 59.4 ka, across the MIS 4/3 transition where prominent shifts in stalagmite δ^{13}C, δ^{18}O, and reflectance occur. No analyses were made during the ~90-yr interval of 60.02–60.11 ka due to a break in the sample section used for trace element analysis. [Sr] for the sampled interval varies between 26 and 76 μg/g, [Ba] between 6 and 28 μg/g, and [Mg] between 800 and 3710 μg/g (Figs. 3 and 4). Stalagmite [Sr] and [Ba] display a strong positive correlation (Table 2) and exhibit shifts that are visually similar to stalagmite δ^{13}C, most notably during the MIS 3 portion of the record younger than ~60 ka. [Mg] displays a weak negative correlation with [Sr] and no correlation with [Ba]. [Mg] also displays a strong positive correlation with δ^{13}C, a moderate positive correlation with δ^{18}O, and a moderate negative correlation with ^{87}Sr/^{86}Sr (Table 2).

Discussion

Interpretation of McLean's Cave proxy records

We interpret the ML-2 isotopic, trace element, and reflectance time-series, to record variations in infiltration, soil respiration, water–rock interaction, temperature and sources of precipitation. Despite multiple influences on each proxy, these records point to significant variations in Sierra Nevada hydroclimate across the MIS 4/3 transition, during D–O cycles 15 through 18, and during additional abrupt millennial-scale events not recorded in NGRIP, but present in other records (e.g. Peterson et al., 2000; Wang et al., 2001; Boch et al., 2011a). For comparison, we use the NGRIP δ^{18}O record plotted on the extended GICC05 chronology of Wolff et al. (2010) (Fig. 5G), which is generally accepted as the standard Greenland ice-core chronology. In this record, the onset of GIS17 and placement of the MIS 4/3 transition has an age of 59.44 ± 1.287 ka (1 σ) (Wolff et al., 2010). We also compare the ML-2 record to absolute dated speleothem records from Hulu Cave in China (Wang et al., 2001) (Fig. 5D), and the Villars Cave and NALPS records from Europe (Genty et al., 2003; Boch et al., 2011a) (Fig. 5E), which display shifts synchronous with D–O events. Correspondence between shifts in the Hulu Cave δ^{18}O record and Greenland interstadials events (GISs) was originally determined against the GISP2 δ^{18}O record, and the estimated error in the GISP2 timescale in this interval is ±10% (Stuiver and Grootes, 2000). Similarly, the age-model for the Cariaco Basin sediment reflectance record (Fig. 5F) has been tuned to the GISP2 timescale during this interval (Peterson et al., 2000), and this may account for the visible offset between the Cariaco Basin and the other records presented in Figure 5.

ML-2 stable isotopes and reflectance display shifts synchronous with interstadial (GISs 15, 16, 17, 18) and stadial events of MIS 4 and 3, that are documented in NGRIP, the Chinese and European stalagmite stable isotope records, and the Cariaco Basin reflectance record (Fig. 5). Transitions in the ML-2 proxy records that we interpret to be associated with GIS 17 occur at 59.8 ± 0.6 ka, within error of shifts in the NGRIP, Hulu, and Villars Cave records (Wang et al., 2001; Genty et al., 2003). Of the ML-2 proxy records, reflectance is most strongly correlated with NGRIP δ^{18}O (r_s = 0.69, p < 0.001) (Table 3). GIS 16 and 17 are each represented by double peaks in the NGRIP δ^{18}O record, and similar structures are also seen in the ML-2 reflectance record. Peaks in ML-2 stable isotopes associated with GIS 16–18 exhibit an average positive shift of 2.4‰ in δ^{13}C and 1.7‰ in δ^{18}O. Increases of 2.1‰ in δ^{13}C and

https://doi.org/10.1016/j.yqres.2014.04.010 Published online by Cambridge University Press

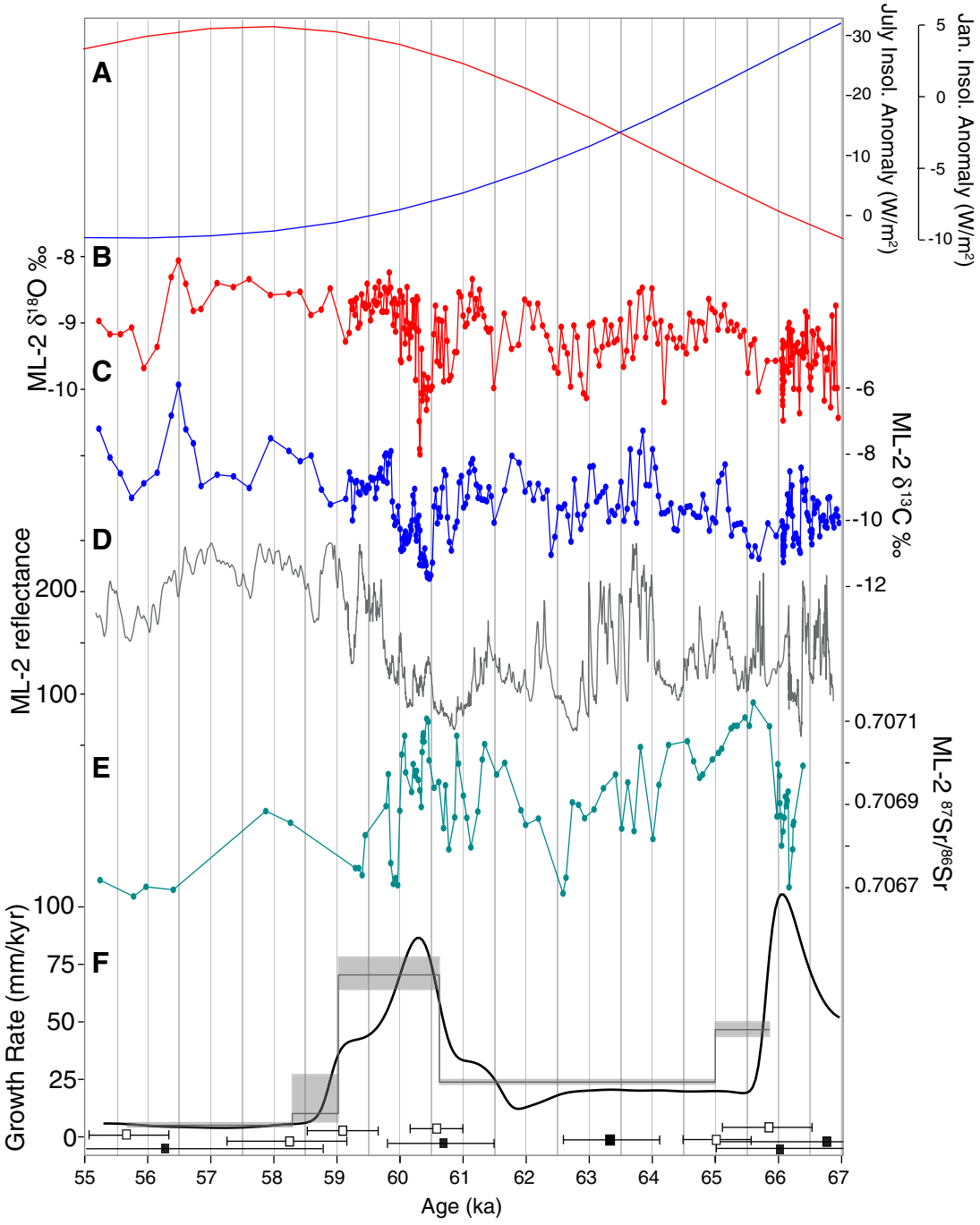

Figure 3. (A) Comparison of January (blue) and July (red) insolation anomalies with $\delta^{18}O$ (B, red), $\delta^{13}C$ (C, blue), reflectance (D, gray), $^{87}Sr/^{86}Sr$ (E, cyan). (F) Stalagmite growth rate. Gray line is the linear rate computed between ICP-MS ages (white boxes near x axis). Gray shading is error on growth rate computed from 2σ errors on ages. Black curve is the growth rate estimated as the first derivative of the StalAge model incorporating both ICP-MS and TIMS ages (black boxes) and then smoothed using a Gaussian kernel smoother with a bandwidth of 0.5.

0.7‰ in $\delta^{18}O$ beginning at 55.7 to 60 ka are synchronous with GIS 15 in the NGRIP record.

The oldest Heinrich Event, H6, occurs during the interval covered by the ML-2 proxy records. Its age is poorly constrained in marine sediment records, but has been estimated as 60 ± 5 ka (Hemming, 2004). Based on comparisons with ice core and speleothem records (Fig. 5), we suggest that climate perturbations relating to H6 began in the central Sierra Nevada at 60.9 ± 0.5 ka, when $\delta^{18}O$ and $\delta^{13}C$ show abrupt negative shifts of 1.5 and 2.1‰ respectively and growth rate substantially increases. H6 lasted ~1100 yr until 59.8 ± 0.6 ka when $\delta^{13}C$ shows an abrupt positive shift of 2.1‰, and growth rate decreases (Figs. 4, 5).

The ML-2 proxy records also display shifts that do not correspond to changes in NGRIP $\delta^{18}O$. These include increases in $\delta^{18}O$ and $\delta^{13}C$ at 56.5 ka just following GIS 16, increases in $\delta^{18}O$, $\delta^{13}C$, and reflectance at 65.2 ka preceding GIS 18, and multiple shifts in $\delta^{18}O$, $\delta^{13}C$, reflectance, and $^{87}Sr/^{86}Sr$ from 63.5 to 60.5 ka between GIS 18 and H6. Many of these shifts in the ML-2 proxy records correspond with changes in the Hulu, Cariaco Basin, and NALPS records, suggesting climate variations occurred in the midlatitudes that were not associated with Greenland temperature change.

In stalagmite ML-2, calcite that formed during Greenland interstadials (GIS 15–18) exhibits higher reflectance and is characterized by

https://doi.org/10.1016/j.yqres.2014.04.010 Published online by Cambridge University Press

Table 2
Spearman rank-order correlation coefficients (r_s values) for ML-2 proxies. Proxy data has been binned where necessary (see text) and linear trends have been removed.

	$\delta^{18}O$	$\delta^{13}C$	$^{87}Sr/^{86}Sr$	Reflectance	Mg	Sr	Ba
$\delta^{18}O$		0.56**	0.3	0.29*	0.68*	−0.02	0.17
$\delta^{13}C$	0.56**		0.04	0.42**	0.78**	0.08	0.31
$^{87}Sr/^{86}Sr$	0.3	0.04		−0.02	−0.62*	−0.09	−0.29
Reflectance	0.29*	0.42**	−0.02		0.12	−0.29**	−0.31**
Mg	0.68*	0.78**	−0.62*	0.12		−0.16**	0.01
Sr	−0.02	0.08	−0.09	−0.29**	−0.16**		0.87**
Ba	0.17	0.31	−0.29	−0.31**	0.01	0.87**	

** $p < 0.001$.
* $p < 0.05$.

open columnar fabrics with abundant porosity along crystallite boundaries and, during GIS 15, laminae of microcrystalline calcite. Calcite that formed during stadials exhibits lower reflectance and consists of columnar calcite in which the crystallites have more completely coalesced leaving fewer inclusions along crystallite boundaries (Supplementary Fig. 2). Variations between open and porous and dense stalagmite crystal fabrics have been linked to changes in drip rate, water film thickness, and calcite supersaturation, as well as changes in cave ventilation. Open columnar calcite fabrics have been related to variable drip rates and $CaCO_3$ supersaturation (Frisia et al., 2000; Frisia and Borsato, 2010; Belli et al., 2013) and reduced water excess (Genty and Quinif, 1996) but also to higher cave air pCO_2 and low drip water pH that promote vertical growth of crystals over lateral coalescence (Boch et al., 2011b). Microcrystalline calcite fabrics are also indicative of variable

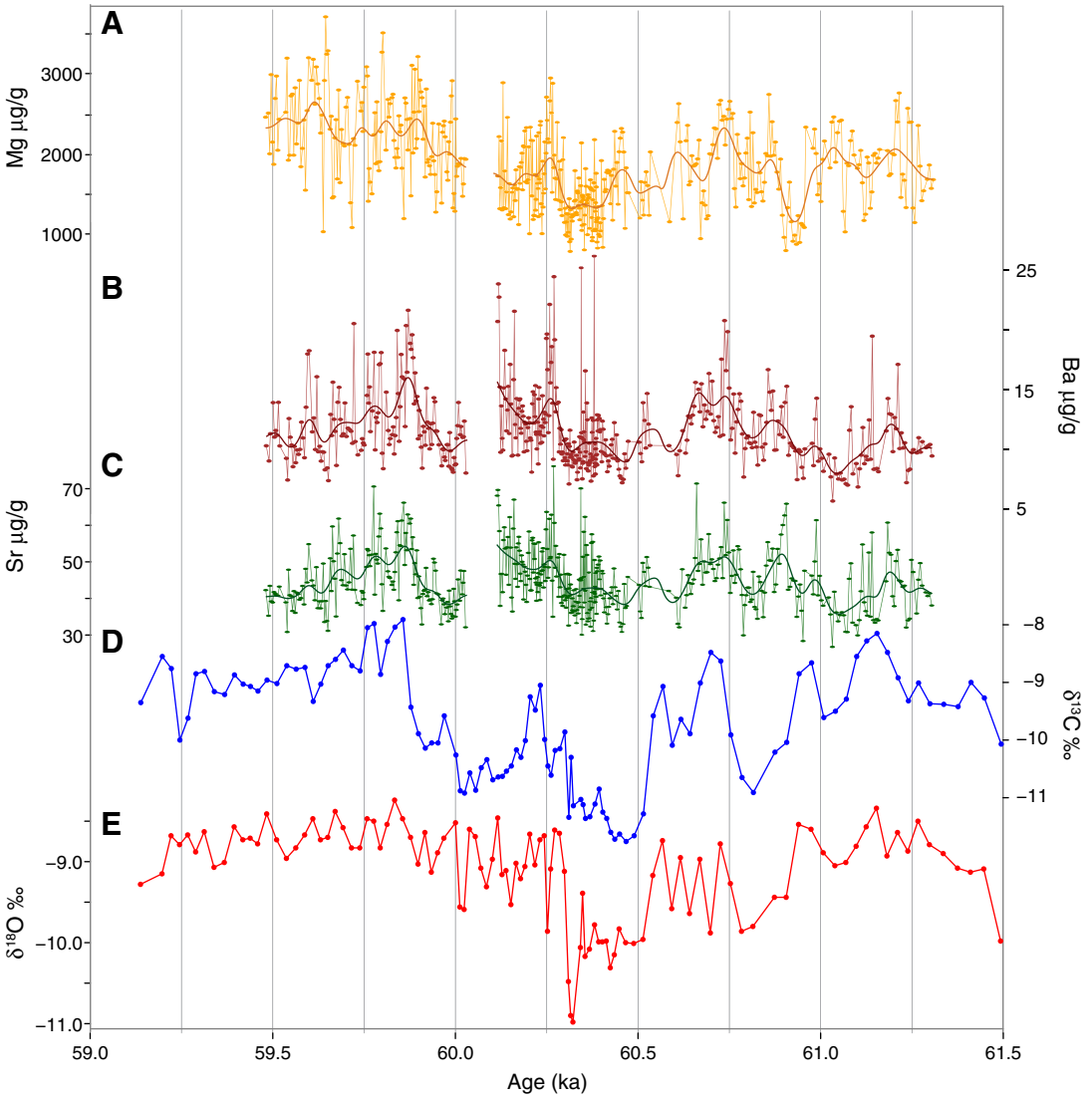

Figure 4. For the period 59.0 to 61.5 ka, records of (A) Mg, (B) Ba, and (C) Sr concentrations in ML-2. Thick solid lines are Gaussian kernel smoothing functions calculated for a bandwidth (h = 0.058) determined by the Sheather Jones method. (D) and (E) show $\delta^{13}C$ and $\delta^{18}O$ records for the same time period. Note gap in elemental concentration records (60.02–60.1 ka) due to sample damage.

https://doi.org/10.1016/j.yqres.2014.04.010 Published online by Cambridge University Press

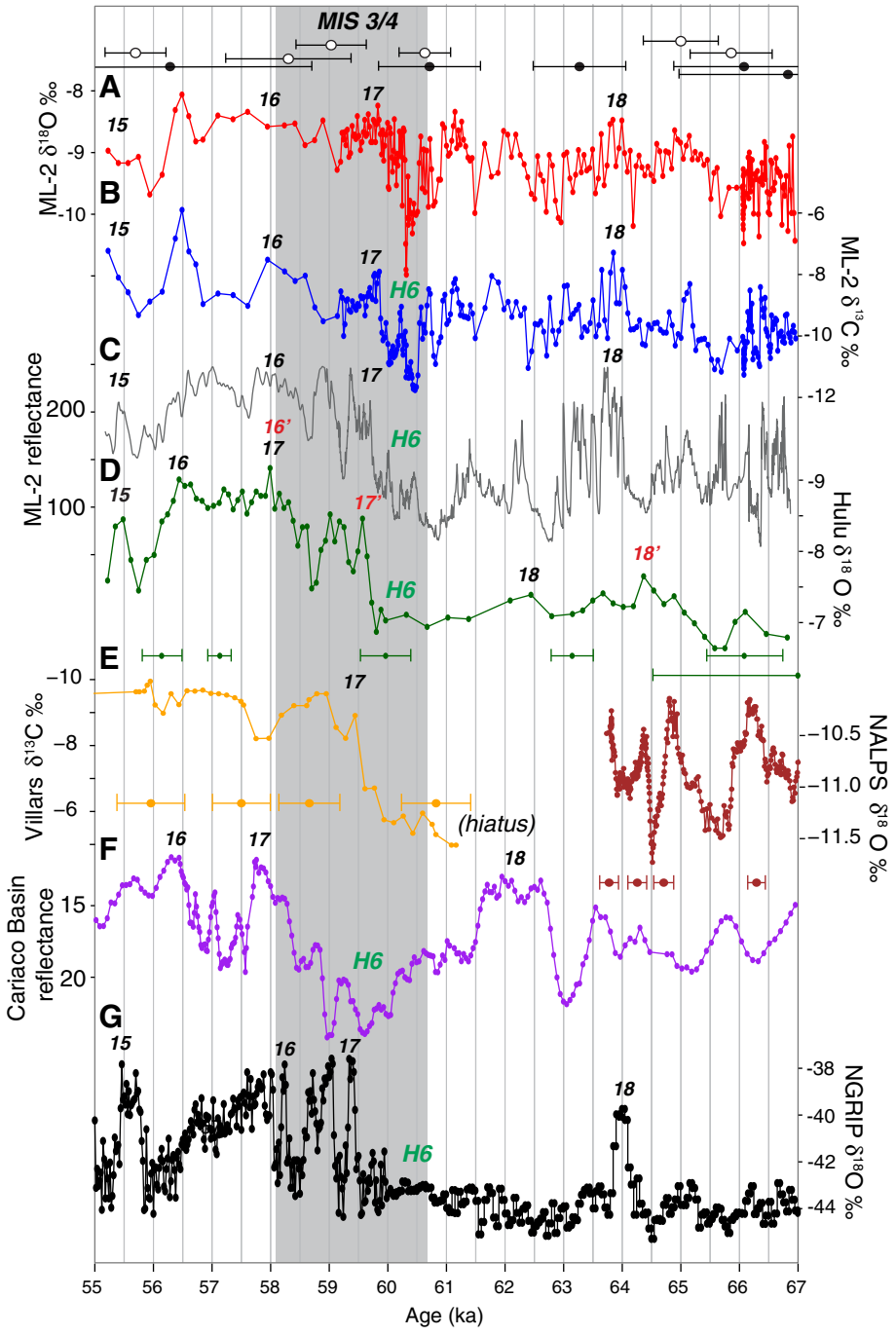

Figure 5. (A) ML-2 $\delta^{18}O$ (red), (B) $\delta^{13}C$ (blue), and (C) reflectance (gray), with $^{230}Th/U$ ages and associated 2σ errors (black circles are TIMS ages, white circles are ICP-MS ages. (D) Hulu Cave $\delta^{18}O$ (y axis is reversed) (Wang et al., 2001) (green), (E) Villars Cave $\delta^{13}C$ (y axis is reversed) (Genty et al., 2003) (orange) and Northern Alps $\delta^{18}O$ (Boch et al., 2011a). $^{230}Th/U$ ages and associated 2σ errors are shown for all speleothem records. (F) Cariaco Basin sediment reflectance (y axis is reversed) (Peterson et al., 2000) (purple); NGRIP ice core $\delta^{18}O$ (NGRIP Members, 2004) on an extended GICC05 timescale (Wolff et al., 2010) derived from shifting the NGRIP record older than 60 ka that is based on the ss09sea chronology forward in time 705 yr to match the onset of GIS 17 in the updated GICC05 chronology (Svensson et al., 2008) (black). The Cariaco Basin chronology has been tuned to the GISP2 ice-core timescale which differs from the more recently constructed NGRIP timescale by ~2 ka in this interval. Greenland Interstadials (GISs) 15–18 are labeled in black on the NGRIP, Cariaco, Villars, and Hulu records according to their original publications. GISs were originally labeled on the Hulu Cave record through comparison with the GISP2 record. A suggested updated labeling of these events based on comparison with NGRIP is shown in red with prime symbols. Timing of Heinrich Event 6 (H6) is labeled in each record in green. Gray bar highlights the MIS4/3 boundary at the onset of GIS 17 as defined by the NGRIP record (59.44 ± 1.287; Wolff et al., 2010).

drip rates and the presence of impurities in the drip water (Frisia and Borsato, 2010). More compact columnar calcite fabrics have been shown to precipitate under moderate, uniform drip rates and low $CaCO_3$ supersaturation (i.e., always wet at the growth site; Frisia et al., 2000; Frisia and Borsato, 2010); increased water excess (Genty and Quinif, 1996), as well as lower cave air pCO_2 (Boch et al., 2011b).

We interpret the more open columnar and microcrystalline fabrics, signified by increased reflectance during Greenland interstadials to suggest variable drip rates and $CaCO_3$ supersaturation. In contrast, the denser columnar crystals, signified by lower reflectance, during stadials are compatible with a steady water supply and more continuous calcite precipitation under low levels of $CaCO_3$ supersaturation.

https://doi.org/10.1016/j.yqres.2014.04.010 Published online by Cambridge University Press

Table 3
Spearman rank-order correlation coefficients (**rs** values) for ML-2 proxies and the Hulu Cave and NGRIP $\delta^{18}O$ records. Proxy data has been binned by 250-yr intervals and linear trends have been removed.

	ML–$\delta^{18}O$	ML–$\delta^{13}C$	ML–reflectance	Hulu–$\delta^{18}O$	NGRIP–$\delta^{18}O$
ML–$\delta^{18}O$		0.51**	0.53**	−0.54**	0.35*
ML–$\delta^{13}C$	0.51**		0.46*	−0.52**	0.16
ML–reflectance	0.53**	0.46*		−0.74**	0.69**
Hulu–$\delta^{18}O$	−0.54**	−0.52**	−0.74**		−0.52**
NGRIP–$\delta^{18}O$	0.35*	0.16	0.69**	−0.52**	

** $p < 0.001$.
* $p < 0.05$.

These interpretations are broadly consistent with long-term changes in ML-2 growth rate, which is generally slower during the MIS 3 portion of the stalagmite (younger than ~60 ka) when calcite fabrics indicate variable water supply, and faster during the MIS 4 portion of the record when fabrics indicate a more continuous water supply (Fig. 3F). However, the rate of calcite precipitation at a speleothem growth site and in the epikarst above the cave (prior calcite precipitation, or PCP) has been shown to respond to both water supply and the pCO_2 gradient between the overlying soil and cave (Banner et al., 2007; Kowalczk and Froelich, 2010; Mattey et al., 2010). Enhanced cave ventilation due to large seasonal temperature differences above the cave would act to lower cave air pCO_2 and increase the soil-to-cave CO_2 gradient (Banner et al., 2007; Kowalczk and Froelich, 2010). Thus changes in the degree of seasonality might lead to variations in ventilation and in turn, changes in speleothem growth rates.

Summer insolation at the latitude of McLean's Cave increases throughout the time period recorded by ML-2, while winter insolation decreases, and from this we infer that seasonality increased through the course of the ML-2 record (Fig. 3A). Ventilation of McLean's Cave was likely elevated during MIS 3 relative to MIS 4, and cave air pCO_2 was likely reduced. However, stalagmite growth rates are slowest between 58.5 and 55 ka during MIS 3 (~3.5 mm/ka), suggesting that potential changes in ventilation between MIS 3 and 4 were not a dominant control on stalagmite growth rate and crystal fabric, in contrast to the relationships observed in Katerloch Cave, Austria (Boch et al., 2011b). We infer that changes in water supply primarily controlled the calcite fabrics displayed by ML-2 and that stadials were characterized by levels of $CaCO_3$ supersaturation and steady water supply due to an overall wetter climate while interstadials were characterized by variable drip rates and episodic supply of water to the cave.

Variations in ML-2 reflectance and average growth rate are accompanied by correlative changes in $\delta^{13}C$, indicating shared environmental controls on these proxies (Table 2). Stadials are characterized by decreased reflectance and more negative speleothem $\delta^{13}C$ values likely reflecting the ^{12}C-enriched soil CO_2 source in seepage waters that is less modified by degassing and PCP compared to interstadials. In regions that are not water limited such as the tropics, temperature is the primary influence on soil respiration rate and soil pCO_2. However, in Mediterranean climates such as the western slope of the Sierra Nevada, soil moisture can provide the primary control on soil respiration rate and pCO_2 (Orchard and Cook, 1983; Quade et al., 1989; Terhune and Harden, 1991; Reichstein et al., 2003). Provided that well developed soils occurred above McLean's Cave, the more negative $\delta^{13}C$ values during stadials could reflect increased soil respiration as a result of increased soil moisture. However, it is also possible that lower temperatures during stadials tempered the effect of increased moisture on soil respiration. Dense columnar calcite textures and the more negative $\delta^{13}C$ values indicate that stadials were characterized by reduced PCP and continuous stalagmite growth facilitated by a steady water supply.

In addition to $\delta^{13}C$, PCP has also been demonstrated to increase trace element concentrations of drip waters and speleothems in the central Sierra Nevada (Oster et al., 2009, 2012). The very strong positive correlation between ML-2 Sr and Ba concentrations (Table 2) suggests that PCP controls these parameters. Although there is no statistically significant relationship between $\delta^{13}C$ and Sr or Ba concentrations (Table 2), there are consistent trends among the data sets, most notably marked increases around 60.4 and 59.8 ka near the MIS 4/3 transition (Fig. 4). The lack of relationship could arise due to the required binning of the trace element data at lower resolution for comparison with $\delta^{13}C$, which could obscure finer-scale relationships between these proxies. However, the marked increases in all records near the MIS 4/3 transition and similar patterns of variability between $\delta^{13}C$, Sr, and Ba concentrations especially during MIS3 (Fig. 4) further indicate that PCP was enhanced in the McLean's Cave system during MIS 3 relative to MIS 4.

Variations in the $^{87}Sr/^{86}Sr$ and Mg concentration of the ML-2 stalagmite are also linked to changes in hydroclimate. These proxies likely reflect varying degrees of dolomite dissolution by seepage waters in the epikarst. The Columbia marble unit that hosts McLean's Cave consists of up to 50% dolomite at the Columbia Quarry near the site of McLean's Cave (Bowen, 1973; C. Haughy, Blue Mountain Minerals, pers. comm. 2010). Slower weathering of dolomite than calcite has been documented within karst systems in the field (Cowell and Ford, 1980; Atkinson, 1983) and experimentally (Chou et al., 1989). Seepage waters tend to reach supersaturation with respect to calcite before they reach dolomite saturation (Roberts et al., 1998), and changes in seepage-water flow rate can cause variations in the amount of dolomite dissolved and seepage-water Mg-content (Fairchild et al., 2000; Hellstrom and McCulloch, 2000). Thus, slower flow rates during dry periods could have led to longer water–rock contact times and waters that were supersaturated with respect to calcite while remaining undersaturated with respect to dolomite.

Given that host dolomite $^{87}Sr/^{86}Sr$ values (0.706773 ± 0.00059) are less radiogenic than host calcite values (0.707233 ± 0.0000090), the overall lower $^{87}Sr/^{86}Sr$ values of the ML-2 stalagmite during MIS 3 (Fig. 3E), coincident with intervals of more open columnar and microcrystalline fabrics signified by higher reflectance and less negative $\delta^{13}C$ is consistent with slower and episodic flow through the epikarst to the drip-site, leading to increased dolomite dissolution during dry periods. Conversely overall more radiogenic stalagmite $^{87}Sr/^{86}Sr$ values during MIS 4, coincident with intervals of dense columnar fabrics signified by lower reflectance and more negative $\delta^{13}C$ are consistent with decreased dolomite dissolution during wet periods when seepage-flow rates through the epikarst were faster and more continuous. The negative correlation between $^{87}Sr/^{86}Sr$ and Mg concentration (Table 2) further supports this relationship.

Host rock limestone has a slightly higher $\delta^{13}C$ value than host rock dolomite (2.22 vs. 1.63 ± 0.03‰, $n = 3$, respectively). Thus, the positive correlation between speleothem $\delta^{13}C$ and Mg concentrations (Table 2) does not indicate that $\delta^{13}C$ is significantly influenced by dolomite dissolution. Rather, this correlation suggests that $\delta^{13}C$ and Mg concentrations are independently controlled by changes in hydroclimate. Taken together, variations in ML-2 reflectance, growth rate, $\delta^{13}C$, trace elements, and $^{87}Sr/^{86}Sr$ indicate that stadials and MIS 4 more broadly were characterized by wetter climates with reduced PCP, less dolomite dissolution

https://doi.org/10.1016/j.yqres.2014.04.010 Published online by Cambridge University Press

and steady water supply to the stalagmite. Conversely interstadials, and MIS 3 more broadly were characterized by drier climates with increased PCP and dolomite dissolution and episodic stalagmite growth that resulted in overall lower growth rates.

Oxygen isotope ratios in speleothems have often been interpreted to reflect changes in the $\delta^{18}O$ of precipitation related to variations in rainfall amount (the "amount effect" of Dansgaard, 1964) (e.g. Wang et al., 2001, 2007; Kanner et al., 2012). However, recent studies have indicated that the source and trajectory of moisture reaching a cave site can have a greater influence on the $\delta^{18}O$ ultimately recorded by speleothem calcite (e.g. Pausata et al., 2011; McCabe-Glynn et al., 2013). We monitored rain and drip water $\delta^{18}O$ at Black Chasm Cavern (BL, Fig. 1B), a tourist cave located 45 km northwest of McLean's Cave and found that rainwater $\delta^{18}O$ is significantly positively correlated with surface air temperature, but shows no significant relationship with rainfall amount (Oster et al., 2012). Additionally we found that changes in moisture source and trajectory do influence the $\delta^{18}O$ of precipitation in the central Sierra Nevada. Storms that originate in the subtropical Pacific have significantly less negative $\delta^{18}O$ values than North Pacific sourced storms (-6.4 ± 2.5‰ versus -15.5 ± 0.4‰) (Oster et al., 2012). This finding is consistent with other regional studies of precipitation and speleothem $\delta^{18}O$ variability (Berkelhammer et al., 2012; McCabe-Glynn et al., 2013).

Given the observed relationships between modern climate conditions and precipitation $\delta^{18}O$, the $\delta^{18}O$ record of the ML-2 stalagmite likely records changes in surface air temperature and variations in the contribution of subtropical water vapor to the central Sierra Nevada. However, speleothem $\delta^{18}O$ can also be influenced by temperature changes at the site of calcite precipitation. Although flooding of the cave precludes measurements of modern internal air temperature variations, temperature has been monitored in other nearby caves. Annual temperature variation within Black Chasm Cavern (BL) is ~1.5 °C (Oster et al., 2012). Temperature variations in Kaweah, Clough, and Soldiers Caves, four wild caves similar in geometry to McLean's Cave (single entrance, vertically oriented) located approximately 240 km to the southwest in Sequoia National Park at elevations of 480, 1260, and 1220 m asl respectively ranged from 0.7 to 1.2 °C over a 2 yr measurement period (2002–2004). If the temperature range of 1.5 °C observed in BL is taken as a likely maximum for temperature variability within McLean's Cave, temperature change would only account for a 0.3‰ change in the $\delta^{18}O$ of speleothem calcite (using the equilibrium fractionation relationship of Kim and O'Neil, 1997). We therefore interpret the ML-2 oxygen isotope values to primarily reflect the drip water $\delta^{18}O$, and thus the $\delta^{18}O$ of precipitation falling above the cave, rather than temperature variability at the site of speleothem deposition (McDermott, 2004).

In addition to surface air temperature and moisture source, the $\delta^{18}O$ of precipitation falling above McLean's Cave during the last glacial cycle was also influenced by changes in continental ice volume that altered the $\delta^{18}O$ of source waters (Dansgaard, 1964; Rozanski et al., 1993). Records from Pacific benthic foraminifera indicate that $\delta^{18}O_{sw}$ decreased by ~0.3‰ across the MIS 4/3 transition (Lisiecki and Raymo, 2009). Such a shift may have slightly attenuated the amplitude of variability recorded by ML-2, as $\delta^{18}O$ in this record increases across this transition. The range of variability across stadial–interstadial transitions in ML-2 (0.7 to 2.5‰) would suggest maximum surface air temperature changes of ~1 to 5 °C, using a mid-latitude relationship of 0.5–0.7‰ per °C change for the $\delta^{18}O$ of precipitation proposed by Rozanski et al. (1993), if no other effects were influencing precipitation $\delta^{18}O$. As described, however, $\delta^{18}O$ variability could also reflect shifts in vapor source to the central Sierra Nevada. It is possible that the proportion of subtropical moisture vapor reaching McLean's Cave increased during interstadials and contributed to increased stalagmite $\delta^{18}O$ during these warmer times. A sustained increase in the frequency of subtropical atmospheric river storms that presently deliver higher $\delta^{18}O$ precipitation to California is predicted to occur in future global-warming scenarios (Dettinger, 2011). If a similar increase in subtropical storms occurred during warmer periods of the past, this would contribute to increased drip water and speleothem $\delta^{18}O$ in central Sierra Nevada caves across the MIS 4/3 transition.

McLean's Cave record and regional climate at the MIS 4/3 transition

Our interpretation of the ML-2 stalagmite record may be compared with existing western North American paleoclimate records of the last glacial period. Stable isotope and trace element records from Owens Lake sediments in east-central California (Li et al., 2004) and a speleothem record from Carlsbad Caverns, New Mexico (Brook et al., 2006) both suggest that wetter conditions prevailed in the southwestern United States during MIS 4 relative to MIS 3, consistent with our findings. The Devils Hole vein calcite exhibits overall lower $\delta^{18}O$ during MIS 4, with a local minimum occurring at ~63.1 ka (±0.64 ka), within dating errors of a period of reduced $\delta^{18}O$, $\delta^{13}C$, and reflectance in the ML-2 stalagmite record. The decrease in the Devils Hole $\delta^{18}O$ record is interpreted to reflect changes in regional $\delta^{18}O_{precip}$ due to decreased SST off the California coast during MIS 4 (Winograd et al., 2006).

Speleothem records document wetter winters during the stadials of MIS 3 in the southwestern US (Asmerom et al., 2010; Wagner et al., 2010). While these stalagmite records begin near the onset of GIS 14, and thus do not overlap with the ML-2 record, our record indicates that the association of interstadials with drier conditions in the western US continued into early MIS 3 and MIS 4, a glacial period but with smaller northern Hemisphere ice sheets relative to MIS 2 (Siddall et al., 2008). In contrast, stable isotope records from four Great Basin lakes suggest that D–O stadials were associated with *drier* conditions in this region between 27 and 50.5 ka (Benson et al., 2003). However, the chronologies for these lake records are complex, based on radiocarbon measurements on lake carbonates and correlation of ash layers and paleomagnetic features between basins (Benson et al., 2003), and some of these correlations may be problematic (Zimmerman et al., 2006). ML-2 proxy records are consistent with variations in foraminiferal assemblages in the Santa Barbara Basin during MIS 3 that suggest stadials off the California coast were associated with decreased SST and increased upwelling, which are attributed to increased northerly winds, a strengthened Aleutian Low, and a southward displaced North Pacific high-pressure cell (Hendy and Kennett, 2000). Strengthening of the Aleutian Low, which is associated with cyclones that pass along the jet stream, would also have led to wetter conditions in the central Sierra Nevada during stadials of MIS 3 and MIS 4.

Paleoclimate records from western North America show some disagreement as to the response of local hydroclimates to Heinrich Events. Pollen from Bear Lake on the Utah–Idaho border suggests Heinrich Events were characterized by cooler and wetter conditions during MIS 2–4 (Jiménez-Moreno et al., 2007), and rock flour abundance in Owens Lake suggests glacial advances occurred in the Sierra Nevada in association with Heinrich Events, including H6 (Bischoff and Cummins, 2001). Many Great Basin lakes reached their most recent highstands during H1 (Munroe and Laabs, 2013), and oxygen and uranium isotope records from Lake Bonneville carbonates suggest wetter conditions prevailed during H2 (McGee et al., 2012). However, $\delta^{18}O$ and TIC records from a Lake Bonneville core indicate drier conditions prevailed during H1–H4 (Benson et al., 2011). Shifts in the ML-2 proxy records during H6 are consistent with others that indicate that wetter conditions prevailed in western North America during Heinrich Events of MIS 2–4.

McLean's Cave record in a global climate context

Comparison of the McLean's Cave proxy records and the Greenland ice core (Fig. 5) suggests generally drier conditions during Greenland Interstadials (GIS 15–18) and wetter conditions during stadials in the Sierra Nevada. At the multi-centennial scale (250 yr time bins), ML-2 reflectance and $\delta^{18}O$ display significant correlations with NGRIP

https://doi.org/10.1016/j.yqres.2014.04.010 Published online by Cambridge University Press

$\delta^{18}O$ (Table 3), while ML-2 $\delta^{13}C$ does not. However, ML-2 reflectance, $\delta^{18}O$, and $\delta^{13}C$ display highly significant negative correlations with the Hulu Cave record of East Asian Monsoon variability (Wang et al., 2001; Cheng et al., 2009). In fact Hulu Cave $\delta^{18}O$ is as strongly negatively correlated with the ML-2 proxy records as it is with NGRIP $\delta^{18}O$ (Table 3). The Cariaco Basin reflectance record, a proxy for changes in productivity that arise from variations in terrestrial sediment input driven by movement of the ITCZ, also displays shifts that are coincident with GIS events during this time period (Fig. 5F) (Peterson et al., 2000). Tuning of the Cariaco Basin record to the GISP2 chronology prevents a robust statistical comparison between it and other proxy records presented in Figure 5. However, the double-trough structure of the H6 event in ML-2 reflectance and stable isotope records, the broad but variable shifts in these parameters associated with GIS18, and the smaller peaks and troughs preceding GIS18 all bear marked resemblance to changes in Cariaco Basin reflectance.

Correlations between ML-2 proxy records and the Hulu Cave and Cariaco Basin records suggest dry conditions in the central Sierra Nevada during Greenland interstadials occurred contemporaneously with an enhanced East Asian (Wang et al., 2001; Liu et al., 2010) or Indian Monsoon (Pausata et al., 2011), and increased river runoff to the Cariaco Basin (Peterson et al., 2000), as well as decreased precipitation in northeastern and southern Brazil (Wang et al., 2004, 2007). The transition from H6 to GIS 17 was also associated with a marked temperature increase in western Europe as documented by the $\delta^{13}C$ record from a Villars Cave stalagmite (Fig. 5E) (Genty et al., 2003). In contrast, wetter conditions in the central Sierra Nevada during stadials were associated with decreased Asian Monsoon intensity, decreased river runoff to the Cariaco Basin, and increased precipitation in northeastern Brazil. Such changes in precipitation in South American and Asian monsoon systems can be explained by shifts in the mean position of the ITCZ in both the Atlantic and the Pacific basins that were coincident with Greenland temperature changes (Wang et al., 2004, 2007; Peterson and Haug, 2006; Clement and Peterson, 2008; Kageyama et al., 2010). Climate models indicate that southward shifts in the ITCZ can be initiated by freshwater input to the North Atlantic leading to slowing of meridional overturning circulation (Vellinga and Wood, 2002; Zhang and Delworth, 2005). A weakening of Atlantic thermohaline circulation has also been shown to lead to a stronger Aleutian low-pressure cell and increased precipitation in western North America (Okumura et al., 2009), as is suggested by the Santa Barbara Basin record for MIS 3 stadials (Hendy and Kennett, 2000). In particular, Heinrich Events provide evidence of freshwater inputs to the North Atlantic through the discharge of icebergs, and thus this mechanism could explain the precipitation increase inferred from the ML-2 proxy records during H6.

Climate models generally do not successfully link the climatic shifts that occur during D–O cycles to changes in thermohaline circulation and, in particular, models have difficulty reproducing the abrupt warming events noted in Greenland temperature records (Clement and Peterson, 2008; Kageyama et al., 2010). In part, this may be attributable to differences in boundary conditions between MIS 3 and the pre-industrial and LGM climates traditionally used in freshwater forcing experiments (Van Meerbeeck et al., 2009). Variations in sea-ice extent may occur on short timescales and could generate the abrupt changes associated with D–O cycles (Li et al., 2005). Models suggest that, under modern boundary conditions, reductions in Arctic sea-ice extent can cause northward-shifted storm tracks and a drier western North America (Sewall and Sloan, 2004; Singarayer et al., 2006). It is possible that changes in sea-ice extent in the Arctic and North Pacific may have contributed to the abrupt shifts in precipitation amount inferred for the central Sierra Nevada during MIS 3 and 4. The inferred decrease in Sierra Nevada precipitation across the MIS 4/3 boundary is also approximately coeval with an increase in eustatic sea level noted in coral and deep-sea records between 60 and 57 ka (Siddall et al., 2008). This suggests that this precipitation decrease may have been associated with a decrease in the size and extent of the Laurentide Ice Sheet that, similar to predictions for Termination I (COHMAP Members, 1988; Bromwich et al., 2004; Kim et al., 2008), may have caused a northward shift in the mean position of the polar jet stream across the MIS 4/3 transition.

Conclusions

High-resolution, U-series dated records of multiple proxies from a stalagmite from McLean's Cave, central California demonstrate that climate there became warmer and drier during the Greenland interstadials associated with D–O events of MIS 4 and early MIS 3 (GISs 15–18), and colder and wetter during Greenland stadials, including Heinrich Event 6. These results are consistent with those from a stalagmite from nearby Moaning Cave, which records a similar relationship between high northern latitude temperatures and Sierra Nevada precipitation between 16.5 and 8.7 ka (Oster et al., 2009), across a similar transition out of glacial conditions. Like the Moaning Cave record, the McLean's Cave records highlight complex interactions between soil respiration, PCP, and water–rock interactions and emphasize the importance of multi-proxy development of speleothem records, especially in semi-arid environments. Despite their complexity, the McLean's Cave stalagmite proxy records provide a reliably dated, continuous, relatively high-resolution snapshot of precipitation variability in western North America during an interval when few such climate records have been developed.

Comparison with global MIS 3 and 4 climate records indicates that the changes in precipitation documented by ML-2 are consistent with migration of the ITCZ and variations in the westerly storm track synchronous with warming in the high northern latitudes. The McLean's Cave record lends support to a growing body of evidence supporting links between high latitude warming and reduced precipitation in western North America.

Supplementary data to this article can be found online at http://dx.doi.org/10.1016/j.yqres.2014.04.010.

Acknowledgments

N.P. Kelley, D.J. Furbish, and J. M. Gilligan provided valuable insight for statistical analyses. C. Haughy provided marble samples from the Columbia Quarry, and B. Rogers assisted in stalagmite collection. G. Barfod was essential in the collection of trace element data. This manuscript benefited from the input of two anonymous reviewers. This work was supported by NSF grants 0823656 (IPM), 0823541 (WDS), and 1203701 (JLO).

References

Asmerom, Y., Polyak, V., Burns, S.J., 2010. Variable moisture in the southwestern United States linked to rapid glacial climate shifts. Nature Geoscience 3, 114–117.
Atkinson, T.C., 1983. Growth mechanisms of speleothems in Castleguard Cave, Columbian Icefields, Alberta, Canada. Arctic Alpine Research 15, 523–526.
Banner, J.L., Guilfoyle, A., James, E.W., Stern, L.A., Musgrove, M., 2007. Seasonal variations in modern speleothem calcite growth in central Texas, U.S.A Journal of Sedimentary Research 77, 615–622.
Belli, R., Frisia, S., Borsato, A., Drysdale, R., Hellstrom, J., Zhao, J.-x., Spötl, C., 2013. Regional climate variability and ecosystem responses to the last deglaciation in the northern hemisphere from stable isotope data and calcite fabrics in two northern Adriatic speleothems. Quaternary Science Reviews 72, 146–158.
Benson, L., Lund, S., Negrini, R., Linsley, B., Zic, M., 2003. Response of North American Great Basin Lakes to Dansgaard–Oeschger oscillations. Quaternary Science Reviews 22, 2239–2251.
Benson, L.V., Lund, S.P., Smoot, J.P., Rhode, D.E., Spencer, R.J., Verosub, K.L., Louderback, L. A., Johnson, C.A., Rye, R.O., Negrini, R.M., 2011. The rise and fall of Lake Bonneville between 45 and 10.5 ka. Quaternary International 235, 57–69.
Berkelhammer, M., Stott, L., Yoshimura, K., Johnson, K., Sinha, A., 2012. Synoptic and mesoscale controls on the isotopic composition of precipitation in the western United States. Climate Dynamics 38, 433–454.
Bischoff, J.L., Cummins, K., 2001. Wisconsin glaciation of the Sierra Nevada (79,000–15,000 yr B.P.) as recorded by rock flour in sediments of Owens Lake, California. Quaternary Research 55, 14–24.
Boch, R., Cheng, H., Spötl, C., Edwards, R.L., Wang, X., Häuselmann, Ph., 2011a. NALPS: a precisely dated European climate record 120–60 ka. Climate of the Past 7, 1247–1259.

Boch, R., Spötl, C., Frisia, S., 2011b. Origin and palaeoenvironmental significance of lamination in stalagmites from Katerloch Cave, Austria. Sedimentology 58, 508–531.
Bowen, O.E., 1973. The Mineral Economics of the Carbonate Rocks: Limestone and Dolomite Resources of California. California Division of Mines and Geology, Sacramento.
Bromwich, D.H., Toracinta, E.R., Wei, H.L., Oglesby, R.J., Fastook, J.L., Hughes, T.J., 2004. Polar MM5 simulations of the winter climate of the Laurentide Ice Sheet at the LGM. Journal of Climate 17, 3415–3433.
Brook, G.A., Ellwood, B.B., Railsback, L.B., Cowart, J.B., 2006. A 164 ka record of environmental change in the American Southwest from a Carlsbad Cavern speleothem. Palaeogeography, Palaeoclimatology, Palaeoecology 237, 483–507.
Cheng, H., Edwards, R.L., Hoff, J., Gallup, C.D., Richards, D.A., Asmerom, Y., 2000. The half-lives of uranium-234 and Thorium-230. Chemical Geology 169, 17–33.
Cheng, H., Edwards, R.L., Broecker, W.S., Denton, G.H., Kong, X., Wang, Y., Zhang, R., Wang, X., 2009. Ice age terminations. Science 326, 248–252.
Chou, K., Garrels, R.M., Wollast, R., 1989. Comparative study of the kinetics and mechanisms of dissolution of carbonate minerals. Chemical Geology 78, 269–282.
Clark, W.B., Lydon, P.A., 1962. Mines and Mineral Resources of Calaveras County, California. California Division of Mines and Geology, San Francisco.
Clement, A.C., Peterson, L.C., 2008. Mechanisms of abrupt climate change of the last glacial period. Reviews of Geophysics 46, RG4002 (2006RG000204).
Cole, K., 1983. Late Pleistocene vegetation of Kings Canyon, Sierra Nevada, California. Quaternary Research 19, 117–129.
Core Team, R., 2012. R: A Language and Environment for Statistical Computing. R Foundation for Statistical Computing, Vienna, Austria 3-900051-07-0 (http://www.R-project.org/).
Cowell, D.W., Ford, D.C., 1980. Hydrochemistry of a dolomite karst: the Bruce Peninsula of Ontario. Canadian Journal of Earth Science 17, 520–526.
Dansgaard, W., 1964. Stable isotopes in precipitation. Telus 16, 436–468.
Dansgaard, W., Johnsen, S., Clausen, H.B., Dahl-Jensen, D., Gundestrup, N., Hammer, C.U., Oeschger, H., 1984. North Atlantic climatic oscillations revealed by deep Greenland ice cores. In: Hansen, J.E., Takahashi, T. (Eds.), Climate Processes and Climate Sensitivity. American Geophysical Union, Washington DC, pp. 288–298.
Davis, O.K., 1999. Pollen analysis of Tulare Lake, California: Great Basin-like vegetation in Central California during the full-glacial and early Holocene. Review of Palaeobotany and Palynology 107, 249–257.
DePaolo, D.J., Ingram, B.L., 1985. High resolution stratigraphy with strontium isotopes. Science 277, 938–941.
Dettinger, D., 2011. Climate change, atmospheric rivers, and floods in California—a multimodel analysis of storm frequency and magnitude changes. Journal of American Water Resources As 47, 514–523.
Fairchild, I.J., Borsato, A.F., Frisia, S., Hawkesworth, C.J., Huang, Y., McDermott, F., Spiro, B., 2000. Controls on trace element (Sr–Mg) compositions of carbonate cave waters: implications for speleothem climatic records. Chemical Geology 166, 255–269.
Frappier, A.B., Sahagian, D., Carpenter, S.J., González, L.A., Frappier, B.R., 2007. Stalagmite stable isotope record of recent tropical cyclone events. Geology 35, 111–114.
Frisia, S., Borsato, A., 2010. Karst. Developments in Sedimentology 61, 269–318.
Frisia, S., Borsato, A., Fairchild, I.J., McDermott, F., 2000. Calcite fabrics, growth mechanisms, and environments of formation in speleothems from the Italian Alps and Southwestern Ireland. Journal of Sedimentary Research 70, 1183–1196.
Genty, D., Quinif, Y., 1996. Annually laminated sequences in the internal structure of some Belgian stalagmites—importance for paleoclimatology. Journal of Sedimentary Research 66, 275–288.
Genty, D., Blamart, D., Ouahdi, R., Gilmour, M., Baker, A., Jouzel, J., Van-Exter, S., 2003. Precise dating of Dansgaard–Oeschger climate oscillations in western Europe from stalagmite data. Nature 421, 833–837.
Harrison, S.P., Sanchez Goñi, M.F., 2010. Global patterns of vegetation response to millennial-scale variability and rapid climate change during the last glacial period. Quaternary Science Reviews 29, 2957–2980.
Heinrich, H., 1988. Origin and consequences of cyclic ice rafting in the northeast Atlantic ocean during the past 130,000 years. Quaternary Research 29, 142–152.
Hellstrom, J.C., McCulloch, M.T., 2000. Multi-proxy constraints on the climatic significance of trace element records from a New Zealand speleothem. Earth and Planetary Science Letters 179, 287–297.
Hemming, S.R., 2004. Heinrich events: massive Late Pleistocene detritus layers of the North Atlantic and their global climate imprint. Review of Geophysics 42, RG1005 (2003RG000128).
Hendy, C.H., 1971. The isotopic geochemistry of speleothems - I. The calculation of the effects of different modes of formation on the isotopic composition of speleothems and their applicability as paleoclimatic indicators. Geochimica et Cosmochimica Acta 35, 801–824.
Hendy, I.L., Kennett, J.P., 2000. Dansgaard–Oeschger cycles and the California Current system: planktonic foraminiferal response to rapid climate change in Santa Barbara Basin, Ocean Drilling Program hole 893A. Paleoceanography 15, 30–42.
Higgins, R.W., Chen, Y., Douglas, A.V., 1999. Interannual variability of the North American warm season precipitation regime. Journal of Climate 12, 653–680.
Holden, N.E., 1990. Total half-lives for selected nuclides. Pure and Applied Chemistry 62, 941–958.
Horwitz, E.P., Chiarizia, R., Dietz, M.L., 1992. A novel strontium-selective extraction chromatographic resin. Solvent Extraction and Ion Exchange 10 (2), 313–336.
Jaffey, A.H., Flynn, K.F., Glendenin, L.E., Bentley, W.C., Essling, A.M., 1971. Precise measurement of half-lives and specific activities of 235U and 238U. Physical Review C 4, 1889–1906.
Jiménez-Moreno, G., Anderson, R.S., Fawcett, P.J., 2007. Orbital- and millennial-scale vegetation and climate changes of the past 225 ka from Bear Lake, Utah–Idaho (USA). Quaternary Science Reviews 26, 1713–1724.
Jo, K., Woo, K.S., Yi, S., Yang, D.Y., Lim, H.S., Wang, Y., Cheng, H., Edwards, R.L., 2014. Mid-latitude interhemispheric hydrologic seesaw over the past 550,000 years. Nature. http://dx.doi.org/10.1038/nature13076.
Jochum, K.P., Weis, U., Stoll, B., Kuzmin, D., Yang, Q., Raczek, I., Jacob, D.E., Stracke, A., Birbaum, K., Frick, D., Günther, G., Enzweiler, J., 2011. Determination of reference values for NIST SRM 610–617 glasses following ISO guidelines. Geostandards and Geoanalytical Research 25, 397–429.
Johnsen, S.J., Clausen, H.B., Dansgaard, W., Fuhrer, K., Gundestrup, N., Hammer, C.U., Iversen, P., Jouzel, J., Stauffer, B., Steffensen, J.P., 1992. Irregular glacial interstadials recorded in a new Greenland ice core. Nature 359, 311–313.
Kageyama, M., Paul, A., Roche, D.M., Van Meerbeeck, C.J., 2010. Modelling glacial climatic millennial-scale variability related to changes in the Atlantic meridional overturing circulation: a review. Quaternary Science Reviews 29, 2931–2956.
Kanner, L.C., Burns, S.J., Cheng, H., Edwards, R.L., 2012. High-latitude forcing of the South American Summer Monsoon during the last glacial. Science 335, 570–573.
Kendall, A.C., Broughton, P.J., 1978. Origin of fabrics in speleothems composed of columnar calcite crystals. Journal of Sedimentary Petrology 48, 519–538.
Kim, S.-T., O'Neil, J.R., 1997. Equilibrium and nonequilibrium oxygen isotope effects in synthetic carbonates. Science 61, 3461–3475.
Kim, S.-J., Crowley, T.J., Erickson, D.J., Govindasamy, B., Duffy, P.B., Lee, B.Y., 2008. High resolution climate simulation of the last glacial maximum. Climate Dynamics 31, 1–6.
Kowalczk, A., Froelich, P.N., 2010. Cave air ventilation and CO2 outgassing by radon-222 modeling: how fast do caves breathe? Earth Planetary Science Letters 289, 209–219.
Li, H.-C., Bischoff, J.L., Ku, T.-L., Zhu, Z.-Y., 2004. Climate and hydrology of the Last Interglaciation (MIS 5) in Owens Basin, California: isotopic and geochemical evidence from core OL-92. Quaternary Science Reviews 23, 49–63.
Li, C., Battisti, D.S., Schrag, D.P., Tziperman, E., 2005. Abrupt climate shifts in Greenland due to displacements of the sea ice edge. Geophysical Research Letters 32, L19702. http://dx.doi.org/10.1029/2005GL023492.
Lisiecki, L.E., Raymo, M.E., 2009. Diachronous benthic $\delta^{18}O$ responses during late Pleistocene terminations. Paleoceangraphy 24. http://dx.doi.org/10.1029/2009PA001732.
Liu, D., Wang, Y., Cheng, H., Edwards, R.L., Kong, X., Wang, X., Hardt, B., Wu, J., Chen, S., Jiang, X., He, Y., Dong, J., Zhao, K., 2010. Sub-millennial variability of Asian monsoon intensity during the early MIS 3 and its analogue to the ice age terminations. Quaternary Science Reviews 29, 1107–1115.
Lorens, R.B., 1981. Sr, Cd, Mn, and Co distribution coefficients in calcite as a function of calcite precipitation rate. Geochimica et Cosmochimica Acta 45, 553–561.
Ludwig, K.R., Wallace, A.R., Simmons, K.R., 1985. The Schwartzwalder uranium deposit, II: age of uranium mineralization and Pb-isotope constraints on genesis. Economic Geology 80, 1858–1871.
Mattey, D.P., Fairchild, I.J., Atkinson, T.C., Latin, J.-P., Ainsworth, M., Durell, R., 2010. Seasonal microclimate control of calcite fabrics, stable isotope, and trace elements in modern speleothem from St. Michaels Cave, Gibraltar. Geological Society of London, Special Publication 336, 323–344.
McCabe-Glynn, S., Johnson, K.R., Strong, C., Berkelhammer, M., Sinha, A., Cheng, H., Edwards, R.L., 2013. Variable North Pacific influence on drought in southwestern North America since AD 854. Nature Geoscience 6, 617–621.
McDermott, F., 2004. Palaeo-climate reconstruction from stable isotope variation in speleothems: a review. Quaternary Science Reviews 23, 901–918.
McEachern, J.M., Grady, M.A., 1978. An inventory and evaluation of the cave resources to be impacted by the New Melones Reservoir Project, Calaveras and Tuolumne Counties, California. Final Report Submitted to the Sacramento District Office of the U.S. Army Corps of Engineers in compliance with Contract DACW05-77-C00038 (102 pp.).
McGee, D., Quade, J., Edwards, R.L., Broecker, W.S., Cheng, H., Reiners, P.W., Evenson, N., 2012. Lacustrine cave carbonates: novel archives of paleohydrologic change in the Bonneville Basin (Utah, USA). Earth and Planetary Science Letters 351–352, 182–194.
Members, C.O.H.M.A.P., 1988. Climatic changes of the last 18,000 years: observations and model simulations. Science 241, 1043–1052.
Mertz-Kraus, R., Sharp, W.D., Ludwig, K.R., 2012. Precise and accurate measurement of U and Th isotopes via ICP-MS using a single solution. Geophysical Research Abstracts 14 (EGU2012-6342, EGU General Assembly 2012).
Mickler, P.J., Banner, J.L., Stern, L., Asmerom, Y., Edwards, R.L., Ito, E., 2004. Stable isotope variations in modern tropical speleothems: evaluating equilibrium vs. kinetic isotope effects. Geochimica et Cosmochimica Acta 68, 4381–4393.
Mickler, P.J., Stern, L.A., Banner, J.L., 2006. Large kinetic isotope effects in modern speleothems. Geological Society of America Bulletin 118, 65–81.
Munroe, J.S., Laabs, B.J.C., 2013. Temporal correspondence between pluvial lake highstands in the southwestern US and Heinrich Event 1. Journal of Quaternary Science 28, 49–58.
North Greenland Ice Core Project members, 2004. High-resolution record of Northern Hemisphere climate extending into the last interglacial period. Nature 431, 147–151.
Okumura, Y.M., Deser, C., Hu, A., Timmermann, A., Xie, S.-P., 2009. North Pacific climate response to freshwater forcing in the subarctic North Atlantic: oceanic and atmospheric pathways. Journal of Climate 22, 1424–1445.
Orchard, V.A., Cook, F.J., 1983. Relationship between soil respiration and soil moisture. Soil Biology and Biochemistry 15, 447–453.
Oster, J.L., Montañez, I.P., Sharp, W.D., Cooper, K.M., 2009. Late Pleistocene California droughts during deglaciation and Arctic warming. Earth and Planetary Science Letters 288, 434–443.
Oster, J.L., Montañez, I.P., Sharp, W.D., Guilderson, T.P., Banner, J.L., 2010. Modeling speleothem $\delta^{13}C$ variability in a Central Sierra Nevada Cave using ^{14}C and $^{87}Sr/^{86}Sr$. Geochimica et Cosmochimica Acta 74, 5228–5524.
Oster, J.L., Montañez, I.P., Kelley, N.P., 2012. Response of a modern cave system to large seasonal precipitation variability. Geochimica et Cosmochimica Acta 91, 92–108.

https://doi.org/10.1016/j.yqres.2014.04.010 Published online by Cambridge University Press

Palmer, M.R., Edmond, J.M., 1989. The strontium isotope budget of the modern ocean. Earth and Planetary Science Letters 92, 11–26.
Pausata, F.S.R., Battisti, D.S., Nisancioglu, K.H., Bitz, C.M., 2011. Chinese stalagmite $\delta^{18}O$ controlled by changes in the Indian monsoon during a simulated Heinrich event. Nature Geoscience 4, 474–480.
Peterson, L.C., Haug, G.H., 2006. Variability in the mean latitude of the Atlantic Intertropical Convergence Zone as recorded by riverine input of sediments to the Cariaco Basin (Venezuela). Palaeogeography, Palaeoclimatology, Palaeoecology 234, 97–113.
Peterson, L.C., Haug, G.H., Hughen, K.A., Röhl, U., 2000. Rapid changes in the hydrologic cycle of the tropical Atlantic during the Last Glacial. Science 290, 1947–1951.
Quade, J., Cerling, T.E., Bowman, J.R., 1989. Systematic variations in the carbon and oxygen isotopic composition of pedogenic carbonate along elevation transects in the southern Great Basin, United States. Geological Society of America Bulletin 101, 464–475.
Rehfeld, K., Marwan, N., Heitzig, J., Kurths, J., 2011. Comparison of correlation analysis techniques for irregularly sampled time series. Nonlinear Processes in Geophysics 18, 389–404.
Reichstein, M., Rey, A., Freibauer, A., Tenhunen, J., Valentini, R., Banza, J., Casala, P., Cheng, Y., Grunzweig, J.M., Irvine, J., Joffre, R., Law, B.E., Loustau, D., Miglietta, F., Oechel, W., Ourcival, J.-M., Pereira, J.S., Peressotti, A., Ponti, F., Qi, Y., Rambal, S., Rayment, M., Romanya, J., Rossi, F., Tedeschi, V., Tirone, G., Xu, M., Yakir, D., 2003. Modeling temporal and large-scale spatial variability of soil respiration from soil water availability, temperature and vegetation productivity indices. Global Biogeochemical Cycles 17. http://dx.doi.org/10.1029/2003GB002035.
Roberts, M.S., Smart, P.L., Baker, A., 1998. Annual trace element variations in a Holocene speleothems. Earth and Planetary Science Letters 154, 237–246.
Rozanski, K., Araguas-Araguas, L., Gonfiantini, R., 1993. Isotopic patterns in modern global precipitation. In: Swart, P.K., et al. (Eds.), Climate change in continental isotope records: American Geophysical Union Monographs, pp. 1–3.
Scholz, D., Hoffmann, D.L., 2011. StalAge—an algorithm designed for construction of speleothem age models. Quaternary Geochronology 6, 369–382.
Scholz, D., Hoffmann, D.L., Hellstrom, J., Ramsey, C.B., 2012. A comparison of different methods for speleothem age modeling. Quaternary Geochronology 14, 94–104.
Sewall, J.O., Sloan, L.C., 2004. Disappearing Arctic sea ice reduces available water in the American west. Geophysical Research Letters 31. http://dx.doi.org/10.1029/2003GL019133.
Sheather, S.J., Jones, M.C., 1991. A reliable data-based bandwidth selection method for kernel density estimation. Journal of the Royal Statistical Society B 53, 683–690.
Siddall, M., Rohling, E.J., Thompson, W.G., Waelbroeck, C., 2008. Marine Isotope Stage 3 sea level fluctuations: data synthesis and new outlook. Reviews in Geophysics 46, RG4003. http://dx.doi.org/10.1029/2007RG000226.
Singarayer, J.S., Bamber, J.L., Valdes, P.J., 2006. Twenty-first-century impacts from a declining Arctic sea ice cover. Journal of Climate 19, 1109–1125.
Sonderegger, D., 2011. SiZer: Significant Zero Crossings. R package version 0.1-4 (http://CRAN.R-project.org/package=SiZer).
Steffensen, J.P., Andersen, K.K., Bigler, M., Clausen, H.B., Dahl-Jensen, D., Fischer, H., Goto-Azuma, K., Hansson, M., Johnsen, S.J., Jouzel, J., Masson-Delmotte, V., Popp, T., Rasmussen, S.O., Röthlisberger, R., Ruth, U., Stauffer, B., Siggaard-Andersen, M.-L., Sveinbjörnsdóttir, A., Svensson, A., White, J.W.C., 2008. High-resolution Greenland ice core data show abrupt climate change happens in few years. Science 321, 680–684.
Stuiver, M., Grootes, P.M., 2000. GISP2 oxygen isotope ratios. Quaternary Research 53, 277–284.
Svensson, A., Andersen, K.K., Bigler, M., Clausen, H.B., Dahl-Jensen, D., Davies, S.M., Johnsen, S.J., Muscheler, R., Parrenin, F., Rasmussen, S.O., Röthlisberger, R., Seierstad, I., Steffensen, J.P., Vinther, B.M., 2008. A 60,000 year Greenland stratigraphic ice core chronology. Climate of the Past 4, 47–57.
Terhune, C.L., Harden, J.W., 1991. Seasonal variations of carbon dioxide concentrations in stony, coarse-textured desert soils of southern Nevada, USA. Soil Science 151, 417–429.
USGS, 2010. United States Geological Survey Preliminary Certificate of Analysis. Microanalytical Carbonate Standard, MACS-3.
Van Meerbeeck, C.J., Renssen, H., Roche, D.M., 2009. How did Marine Isotope Stage 3 and Last Glacial Maximum climates differ? Perspectives from equilibrium simulations. Climate of the Past 5, 33–51.
Vellinga, M., Wood, R.A., 2002. Global climatic impacts of a collapse of the Atlantic thermohaline circulation. Climate Change 54, 251–267.
Voelker, A.H.L., workshop participants, 2002. Global distribution of centennial-scale records for Marine Isotope Stage (MIS) 3: a database. Quaternary Science Reviews 21, 1185–1212.
Wagner, J.D.M., Cole, J.E., Beck, J.W., Patchett, P.J., Henderson, G.M., Barnett, H.R., 2010. Moisture variability in the southwestern United States linked to abrupt glacial climate change. Nature Geoscience 3, 110–113.
Wang, Y.J., Cheng, H., Edwards, R.L., An, Z.S., Wu, J.Y., Shen, C.-C., Dorale, J.A., 2001. A high-resolution absolute-dated Late Pleistocene monsoon record from Hulu Cave, China. Science 294, 2345–2348.
Wang, X., Auler, A.S., Edwards, R.L., Cheng, H., Cristalli, P.S., Smart, P.L., Richards, D.A., Shen, C.-C., 2004. Wet periods in northeastern Brazil over the past 210 kyr linked to distant climate anomalies. Nature 432, 740–743.
Wang, X., Auler, A.S., Edwards, R.L., Cheng, H., Ito, E., Wang, Y., Kong, X., Solheid, M., 2007. Millennal-scale precipitation changes in southern Brazil over the past 90,000 years. Geophysical Research Letters 34. http://dx.doi.org/10.1029/2007GL031149.
Winograd, I.J., Landwehr, J.M., Coplen, T.B., Sharp, W.D., Riggs, A.C., Ludwig, K.R., Kolesar, P.T., 2006. Devils Hole, Nevada, $\delta^{18}O$ record extended to the mid-Holocene. Quaternary Research 66, 202–212.
Wolff, E.W., Chappellaz, J., Blunier, T., Rasmussen, S.O., Svensson, A., 2010. Millennial-scale variability during the last glacial: the ice core record. Quaternary Science Reviews 29, 2828–2838.
Zhang, R., Delworth, T.L., 2005. Simulated tropical response to a substantial weakening of the Atlantic thermohaline circulation. Journal of Climate 18, 1853–1860.
Zimmerman, S.H., Hemming, S.R., Kent, D.B., Searle, S.Y., 2006. Revised chronology for late Pleistocene Mono Lake sediments based on paleointensity correlation to the global reference curve. Earth and Planetary Science Letters 252, 94–106.

https://doi.org/10.1016/j.yqres.2014.04.010 Published online by Cambridge University Press